Molecular Additives Improve Selectivity of CO_2 Photoelectrochemical Reduction over Gold Nanoparticles on Gallium Nitride

Aisulu Aitbekova[1], Nicholas B. Watkins[2], Matthias H. Richter[3], Phillip R. Jahelka[1], Jonas C. Peters[2], Theodor Agapie[2], Harry A. Atwater[1]

[1]Applied Physics and Materials Science, California Institute of Technology, Pasadena, 91125, CA, USA
[2]Chemistry and Chemical Engineering, California Institute of Technology, Pasadena, 91125, CA, USA
[3]Division of Engineering and Applied Science, California Institute of Technology, Pasadena, 91125, CA, USA

Abstract

Photoelectrochemical CO_2 reduction (CO_2R) is an appealing solution to convert carbon dioxide into higher-value products. However, CO_2R in aqueous electrolytes suffers from poor selectivity due to the competitive hydrogen evolution reaction dominant on semiconductor surfaces in aqueous electrolytes. We demonstrate that functionalizing gold/p-type gallium nitride devices with a film derived from diphenyliodonium triflate suppresses hydrogen generation from 90% to 18%. As a result, we observe an increase in the Faradaic efficiency and partial current density for carbon monoxide by 50% and 3x, respectively. Furthermore, we demonstrate through optical absorption measurements that the molecular film employed herein, regardless of thickness, does not affect the photocathode's light absorption and, therefore, photocurrent. Together, this study provides a rigorous platform to elucidate catalytic structure-property relationships to enable engineering of active, stable, and selective materials for photoelectrochemical CO_2 reduction.

TOC

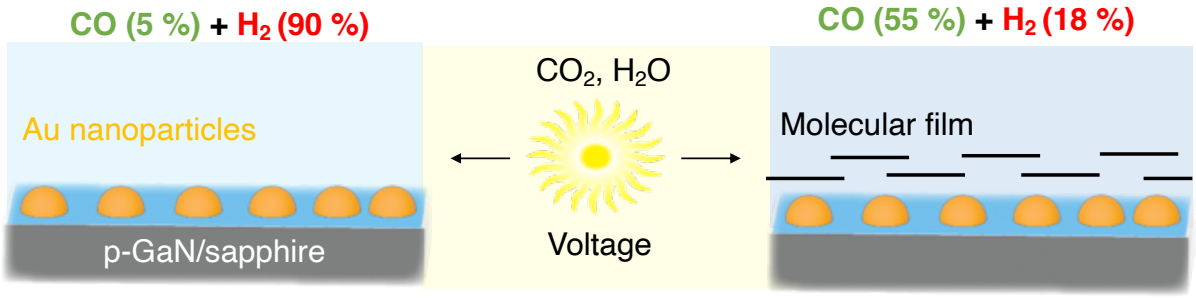

Main text

Photoelectrochemical (PEC) CO_2 reduction (CO_2R) is an appealing strategy to harness abundant solar energy and convert a greenhouse gas into value-added products.[1, 2] Various PEC CO_2R approaches have been demonstrated with planar wide bandgap semiconductors, such as titania and p-type gallium nitride (p-GaN) due to their stability.[3-5] Compared to nanostructured photocathodes, planar substrates offer several advantages, including ease of fabrication and scale-up. However, they display low selectivity for CO_2R.[3, 4] When combined with metals, such as gold, electron-hole separation at the metal-semiconductor interface is enhanced due to the downward bending of the conduction and valence bands.[5, 6] Despite showing improved performance, these systems still require significant optimization and mechanistic studies to drive forward their future application.

Previous research in our group has focused on plasmon-driven CO_2R of metal nanoparticles.[5, 7] We have shown that plasmon-driven PEC CO_2R with the Au/p-GaN photocathodes improved CO production over the hydrogen evolution reaction (HER) in aqueous electrolytes compared to dark electrolysis conditions.[5] However, due to the relatively small contribution of the plasmonic effect (current density on the order of $1\mu A/cm^2$), electrolysis had to be performed in an accumulation mode. To achieve higher current densities, ultraviolet (UV) light can be used to excite carriers in p-GaN via interband absorption. This aspect is particularly important in the context of the practical operation of such devices under natural sunlight. Although the wide bandgap (3.4 eV) limits the solar cell efficiency to 1.7 %, p-GaN shows exceptional stability and can even be used as a protective coating.[6, 8] Regardless of whether GaN is used as a single photoabsorber or a protective coating layer, the semiconductor/electrolyte interface has a significant impact of the performance of photoelectrochemical reduction reactions.[3, 4, 9] To understand how the interband absorption in p-GaN affects its catalytic reactivity, we fabricate p-GaN and Au/p-GaN devices with well-defined properties (size, optical absorption, Schottky barrier height) and study the PEC CO_2R performance of these devices under the full spectrum light illumination. Furthermore, to suppress HER in aqueous electrolytes, we functionalized the surface of p-GaN and Au/p-GaN with films derived from molecular additives akin to our previous studies of film-modified copper[10, 11], silver[12], and chalcopyrite $Cu(In,Ga)Se_2$ semiconductors.[13] Critically, we evaluate how functionalizing the photocathodes with molecular films alters the light absorption of the photoabsorber and, thereby inform future organic-film-modified PEC system design. Finally, demonstrate how film thickness alters the photoabsorber's optical absorption properties and subsequent CO_2 PEC performance.

Our efforts started by characterizing bare p-GaN. We used commercially available p-GaN wafers on sapphire substrates (c-axis 0001 orientation). Optically transparent p-GaN has an absorption step at 365 nm (Figure S1a), consistent with the expected bandgap of 3.4 eV. We observe fringes in the absorption spectra due to Fabry-Pérot interferences within the GaN/sapphire layer and a negative slope in the Mott-Schottky plot, consistent with p-type conductivity[5] **(**Figure S1b**).** Hall measurements yield a carrier concentration of $8*10^{17}$ cm^{-3}, as expected based on the manufacturer's specifications **(**Table S1**).** Having characterized the properties of the bare semiconductor, we fabricated Au/p-GaN devices (Figure 1a) (for details, see the Methods section in Supporting Information). The device consists of a front ohmic nickel-gold (Ni/Au) contact and

gold nanoparticles made via electron-beam physical vapor deposition. Our previous work[5, 14, 15] demonstrates that the nanoparticles form a Schottky contact with the underlying semiconductor substrate with the downward band bending of the conduction and valence bands (Figure 1b). Annealing in the air at 300 °C yielded Au nanoparticles with an average size of 10 nm, as determined by scanning electron microscopy (SEM) characterization **(**Figure 1c**).** The nanoparticles exhibit a clear absorption peak in the visible region at about 570 nm due to the surface plasmon resonance of Au **(**Figure 1d**).** The size of the gold nanoparticles was chosen to ensure the light absorption by p-GaN. The similar absorption values above the semiconductor's bandgap (< 365 nm) confirm that the light effectively interacts with the p-GaN substrate. X-ray photoelectron spectroscopy (XPS) measurements show the metallic state of gold, indicated by the Au 4f5/2 and Au 4f7/2 binding energies of 87.6 and 84 eV, respectively **(**Figure S2**).** The formation of the Ni/Au ohmic and Au Schottky contact is confirmed by solid-state current-voltage measurements (Figure 1e). Finally, working photoelectrodes were made by connecting the Ni/Au ohmic contact to metallic wires using a silver paste and UV-resistant epoxy **(**Figure S3**)**.

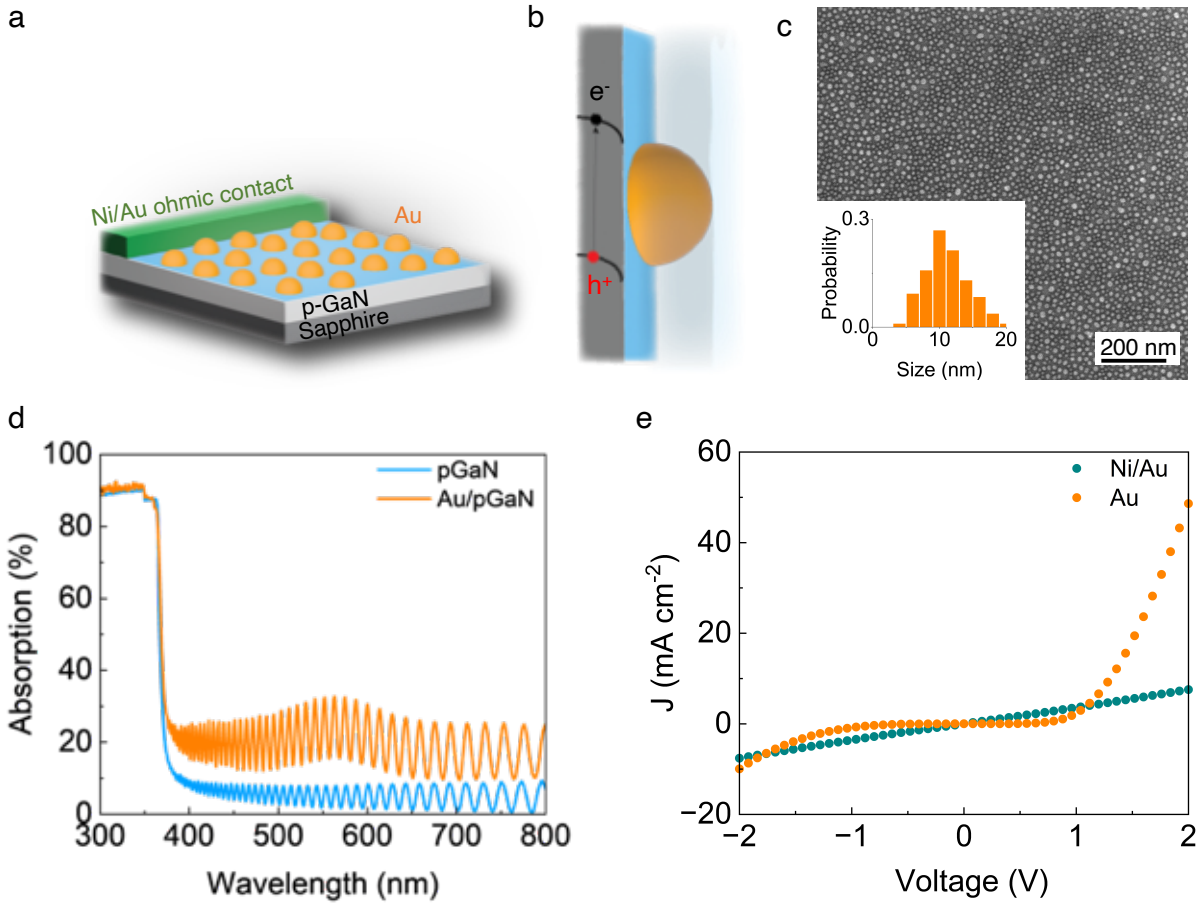

Figure 1. a) Schematic of the Au/p-GaN device; b) Schematic of the Au/p-GaN band diagram with the downward band bending of the conduction and valence bands; c) Representative SEM image and particle size distribution of Au/p-GaN after annealing at 300 °C; d) Optical absorption

of p-GaN and Au/p-GaN; e) Solid-state current-voltage measurements of the Ni/Au ohmic and Au Schottky contacts.

Photoelectrochemical characterization of p-GaN and Au/p-GaN was performed in a 0.1 M $KHCO_3$ solution (pH = 6.8) in the dark and under full-spectrum light illumination by a mercury-xenon lamp (300 mW/cm^2). A three-electrode compression cell used in this study was fabricated according to the previously reported work.[16] All electrochemical potentials are reported with respect to the reversible hydrogen electrode (RHE). It is important to note that a proper ohmic contact is critical to achieving a low solution resistance. Specifically, using a metal foil or an alligator clip gives a solution resistance on the order of 1 kΩ, as measured by potentiostatic electrochemical impedance spectroscopy. In comparison, samples with the Ni/Au ohmic contact have a solution resistance of 30 Ω (Figure S4). Characterization of bare p-GaN under the open-circuit potential further confirms the p-type doping of the semiconductor, as evidenced by the positive shift in V_{oc} upon light exposure (Figure S5). Linear sweep voltammetry (LSV) measurements under periodic full-spectrum light illumination show that p-GaN has negligible activity in the dark but a pronounced photocurrent under illumination due to the inter-band excitation in p-GaN (Figure 2a). Having characterized the bare p-GaN, we investigated the catalytic performance of Au/p-GaN. Similar to p-GaN, Au/p-GaN has a negligible dark current density (Figure 2a). These reported values are based upon geometric current densities. The plasmonic effect has a negligible contribution to the photocurrent density (-0.4 μA cm^{-2} under visible light illumination versus -0.3 μA cm^{-2} in dark, Figure S6), demonstrating that the photocurrent of Au/p-GaN under the full spectrum illumination is dominated by the interband absorption in p-GaN and further highlights the difference between this work and the previous report[5] from our group. Under the full-spectrum illumination, however, the device has a more negative current density than bare p-GaN due to the presence of the gold co-catalyst.

We have also conducted chronoamperometry (CA) measurements to examine the effects of the interband absorption in p-GaN on the selectivity of the CO_2 reduction process. Gold is known to produce carbon monoxide (CO) and hydrogen (H_2) as the major products under CO_2 reduction conditions.[17] For the CA measurements, we chose an applied potential of –0.2 V, which corresponds to the equilibrium CO_2/CO redox potential at pH 6.8 and under which the samples have negligible activity in dark (Figure 2a). Under full-spectrum light illumination, both samples produce H_2 and CO, with H_2 being the dominant product with a Faradaic Efficiency (FE) of 95 and 90% on p-GaN and Au/p-GaN, respectively (Figure 2b). No photocorrosion products were detected using inductively coupled plasma mass spectrometry (Table S2), further highlighting the stability of p-GaN. These results show that HER is primarily driven by p-GaN, consistent with previously reported studies on bulk semiconductor electrodes acting as HER catalysts[18] and underscoring the challenge of facilitating selective CO_2 reduction.

In our previous work, a higher CO/H_2 generation ratio on Au/p-GaN was achieved under dark and visible light illumination conditions due to a sufficiently negative potential (-1.8 V vs RHE) being applied to drive CO_2R on the gold nanoparticles, which is known to favor CO generation over HER, albeit at small current densities. Herein, we employ full spectrum illumination and a significantly lower applied potential (-0.2 V vs RHE), under which the samples

have negligible activity in dark, to investigate Au/p-GaN's reactivity. We demonstrate a much higher photocurrent densities (on the order of 100 μA cm^{-2}) driven by the interband absorption in the p-GaN rather than the plasmonic effect (Figure S6).

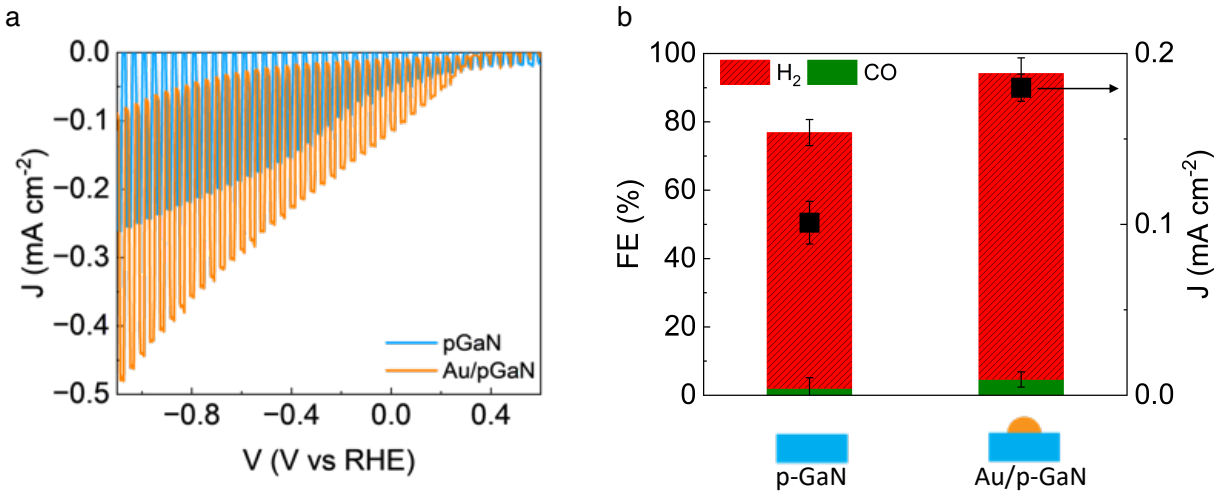

Figure 2. a) Linear sweep voltammograms of p-GaN (blue curve) and Au/p-GaN (orange curve) under periodic full-spectrum light illumination by the Hg-Xe lamp (300 mW/cm^2); b) Faradaic Efficiency (bar graphs) and corresponding current density (black squares) of p-GaN and Au/p-GaN under full-spectrum light illumination at –0.2 V vs RHE.

One approach to enhance selectivity towards carbon products in CO_2R is by functionalizing electrodes with organic coatings.[11, 12, 19-25] Such functionalization can be achieved by dissolving molecular additives in the electrolyte followed by reductive deposition of a film derived from the additives (via a reductive coupling process) onto the surface of the electrodes under an applied potential.[10-13, 26, 27] Herein, we investigated the effect of diphenyliodonium triflate (**Add**, Figure 3) on catalysis, as its polyaromatic thin films have been shown to be stable even under harsh conditions such as pH 1 electrolytes[10] or under UV irradiation[28] (Figure 3). Furthermore, this additive was chosen as it has been shown to be provide films that do not appreciably change the electrochemical active surface area.[10, 20, 28] On copper, the polyaromatic film has been suggested to improve CO_2 reduction performance by suppressing proton transport, and therefore HER. Inspired by these studies, we sought to explore the effects of this molecular additive on improving the CO_2 reduction selectivity of Au/p-GaN.

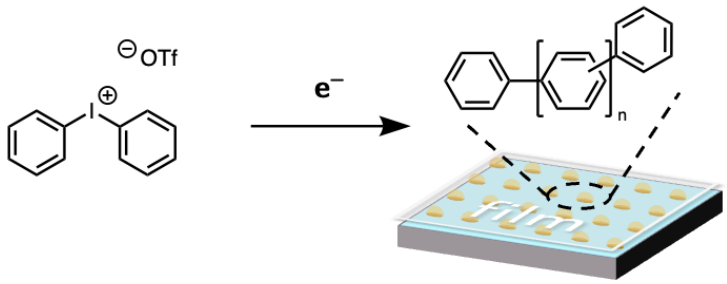

Figure 3. The reductive electropolymerization of diphenyliodonium triflate affords a polyaromatic film on the photoelectrode surface. *In-situ* deposition was performed by using molecular additive solutions (10 mM in 0.1 M $KHCO_3$ electrolyte solution).

Initial CA experiments with Au/p-GaN at –0.2 V RHE under light illumination show that the addition of **Add** increases the FE of CO (from ≤ 5 to 55%) and decreases the FE of H_2 (from ≥ 90 to 18%). While the total current density decreases in the presence of the film, the partial current density for CO increases by 3x (Figure 4a) compared to the bare Au/p-GaN sample. We speculate that this increase in activity can be attributed to the liberated active sites in the absence of HER and potentially increased CO_2 concentration within the films, as suggested previously.[10] As a control experiment, we conducted CA measurements under full-spectrum light irradiation on Au/p-GaN with **Add** under an argon flow (Figure S7). Negligible FE to CO in argon confirms that this product is formed due to enhanced PEC CO_2R and not film decomposition. Interestingly, the ca. 3-fold decrease in the total current density correlates with the total area of the gold nanoparticles constituting 35% of the Au/p-GaN photocathode area. It is important to note that the total FE of Au/p-GaN in the presence of the additives is lower than that of bare Au/p-GaN. This likely results from reduction of the additive during PEC CO_2R.[13]

SEM characterization of the post-electrolysis samples was performed to help understand the structure of Au/p-GaN in the presence of the additive film. Firstly, no sintering of Au nanoparticles was observed (Figure S8). Secondly, we observe a film on the surface of Au/p-GaN with *in-situ* deposited **Add** (sample labelled as 40-Add/Au/pGaN where 40 is the deposition time in minutes), confirming its polymerization under the PEC CO_2R conditions (Figure S9a). The average film thickness as determined from cross-sectional SEM images is ca. 500 nm (Figure S9b). To determine how the film alters the CO_2 PEC performance of the p-GaN substrate, we performed electrolysis with p-GaN in the presence of **Add** under the same reductive bias. Strikingly, HER was completely suppressed (Figure 4a). XPS of the post-catalysis sample shows an absence of the Ga 2p and N 1s peaks associated with the substrate, corroborating the film's deposition and thickness exceeding the electron escape depth of 10 nm (Figure S10).[29]

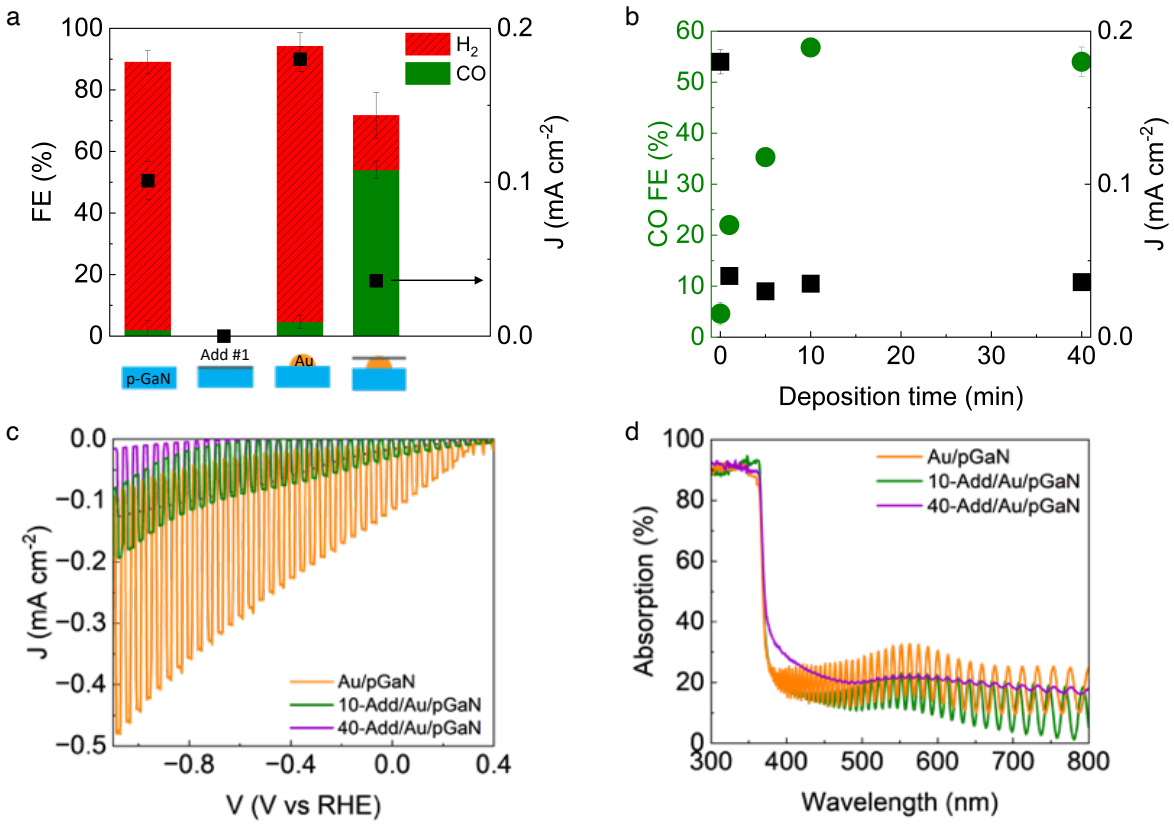

Figure 4. a) Faradaic efficiency (FE) of p-GaN and Au/p-GaN with and without in-situ deposited **Add** under light illumination at -0.2 V vs RHE (bar graphs, left y-axis) and corresponding current density (black squares, right y-axis); b) CO FE (green circles) and current density (black squares) of Au/p-GaN at -0.2 V vs RHE under illumination versus deposition time of **Add**; c-d) Linear sweep voltammograms and optical absorption of unmodified Au/p-GaN, 10-min pre-deposited, and 40-min deposited Add on Au/p-GaN under periodic full-spectrum light illumination.

To further study the effects of film thickness, **Add** was pre-deposited for 1, 5, and 10 min under standard catalytic conditions and then fresh electrolyte was introduced for PEC CO_2R performance evaluation. Each pre-deposition experiment was performed with a new Au/p-GaN sample. In these experiments, we observed a steady increase in the CO selectivity and partial current density as a function of the deposition time (Figure 4b). However, we also find that the CO selectivity saturates as ca. 55 % after 10 min deposition, while the current density remains the same independent of the deposition time. To get a deeper understanding of how the additive film alters the optical properties of Au/p-GaN, we performed additional characterization of the unmodified and the best-performing film-coated Au/p-GaN samples (10-Add/Au/pGaN and 40-Add/Au/pGaN). Average film thicknesses for these samples are ca. 100 and 500 nm, respectively (Figure S11). LSV measurements under periodic full-spectrum light illumination show the decreased photocurrent of the film-coated samples compared to unmodified Au/p-GaN (Figure 4c). However, this decrease is due to the suppressed HER rates of the modified Au/p-GaN devices and not due to the diminished light absorption. To confirm that the films still enable the light absorption by the p-GaN, we have measured optical absorption properties of the same film-coated

samples. While the amplitude of the Fabry-Pérot interferences within the GaN/sapphire layer is damped in the functionalized samples, the similar absorption values above the p-GaN bandgap (< 365 nm) indicates that the film does not attenuate the UV light absorption by the semiconductor, regardless of film thickness (Figure 4d). The decrease in the amplitude of Fabry-Pérot interference fringes in the coated samples is due to enhanced light scattering by the films.

Overall, this work establishes a platform to elucidate structure-property relationships in PEC CO_2R. By fabricating Au/p-GaN devices with well-defined properties (size, optical absorption, Schottky barrier height), we have studied the effects of the interband absorption in p-GaN on its photoelectrochemical CO_2 reduction performance. We show that functionalizing Au/p-GaN with a diphenyliodonium triflate-derived molecular film suppresses HER formation by 72% FE and increases CO partial current density by 3x. Furthermore, we demonstrate that the additive film completely suppresses all HER on bare GaN, suggesting that all reactivity from Au/p-GaN came from the gold nanoparticles. Finally, we reveal that modification of the surface does not attenuate the UV light absorption, thus informing the design and improvement of future photoelectrochemical CO_2R devices.

Acknowledgements

This material is based on work performed by the Liquid Sunlight Alliance, which is supported by the U.S. Department of Energy, Office of Science, Office of Basic Energy Sciences, Fuels from Sunlight Hub under Award Number DE-SC0021266. Part of this work was carried out at the Molecular Materials Research Center in the Beckman Institute of the California Institute of Technology. The Resnick Sustainability Institute is acknowledged for support of enabling facilities at Caltech. We thank Yungchieh Lai for performing ICP-MS measurements. We also thank Azhar Carim for helping collect cross-sectional SEM data. A.A. acknowledges support from the Kavli Nanoscience Institute Postdoctoral Fellowship.

References

(1) Shaner, M. R.; Atwater, H. A.; Lewis, N. S.; McFarland, E. W. A comparative technoeconomic analysis of renewable hydrogen production using solar energy. *Energy Environ. Sci.* **2016**, *9* (7), 2354-2371, 10.1039/C5EE02573G. DOI: 10.1039/C5EE02573G.
(2) Holmes-Gentle, I.; Tembhurne, S.; Suter, C.; Haussener, S. Kilowatt-scale solar hydrogen production system using a concentrated integrated photoelectrochemical device. *Nat. Energy* **2023**, *8* (6), 586-596. DOI: 10.1038/s41560-023-01247-2.
(3) Kan, M.; Wang, Q.; Hao, S.; Guan, A.; Chen, Y.; Zhang, Q.; Han, Q.; Zheng, G. System Engineering Enhances Photoelectrochemical CO_2 Reduction. *J. Phys. Chem. C* **2022**, *126* (4), 1689-1700. DOI: 10.1021/acs.jpcc.1c10156.
(4) Chu, S.; Ou, P.; Ghamari, P.; Vanka, S.; Zhou, B.; Shih, I.; Song, J.; Mi, Z. Photoelectrochemical CO_2 Reduction into Syngas with the Metal/Oxide Interface. *J. Am. Chem. Soc.* **2018**, *140* (25), 7869-7877. DOI: 10.1021/jacs.8b03067.
(5) DuChene, J. S.; Tagliabue, G.; Welch, A. J.; Cheng, W.-H.; Atwater, H. A. Hot Hole Collection and Photoelectrochemical CO_2 Reduction with Plasmonic Au/p-GaN Photocathodes. *Nano Lett.* **2018**, *18* (4), 2545-2550. DOI: 10.1021/acs.nanolett.8b00241.
(6) Zhou, B.; Ou, P.; Pant, N.; Cheng, S.; Vanka, S.; Chu, S.; Rashid, R. T.; Botton, G.; Song, J.; Mi, Z. Highly efficient binary copper−iron catalyst for photoelectrochemical carbon dioxide reduction toward methane. *PNAS* **2020**, *117* (3), 1330-1338. DOI: 10.1073/pnas.1911159117.
(7) DuChene, J. S.; Tagliabue, G.; Welch, A. J.; Li, X.; Cheng, W.-H.; Atwater, H. A. Optical Excitation of a Nanoparticle Cu/p-NiO Photocathode Improves Reaction Selectivity for CO_2 Reduction in Aqueous Electrolytes. *Nano Lett.* **2020**, *20* (4), 2348-2358. DOI: 10.1021/acs.nanolett.9b04895.
(8) Dong, W. J.; Navid, I. A.; Xiao, Y.; Lee, T. H.; Lim, J. W.; Lee, D.; Jang, H. W.; Lee, J.-L.; Mi, Z. Bi catalysts supported on GaN nanowires toward efficient photoelectrochemical CO_2 reduction. *J. Mater. Chem. A* **2022**, *10* (14), 7869-7877, 10.1039/D2TA00032F. DOI: 10.1039/D2TA00032F.
(9) Zeng, G.; Pham, T. A.; Vanka, S.; Liu, G.; Song, C.; Cooper, J. K.; Mi, Z.; Ogitsu, T.; Toma, F. M. Development of a photoelectrochemically self-improving Si/GaN photocathode for efficient and durable H_2 production. *Nat. Mater.* **2021**, *20* (8), 1130-1135. DOI: 10.1038/s41563-021-00965-w.
(10) Watkins, N. B.; Wu, Y.; Nie, W.; Peters, J. C.; Agapie, T. In Situ Deposited Polyaromatic Layer Generates Robust Copper Catalyst for Selective Electrochemical CO_2 Reduction at Variable pH. *ACS Energy Lett.* **2023**, *8* (1), 189-195. DOI: 10.1021/acsenergylett.2c02002.
(11) Han, Z.; Kortlever, R.; Chen, H.-Y.; Peters, J. C.; Agapie, T. CO_2 Reduction Selective for C≥2 Products on Polycrystalline Copper with N-Substituted Pyridinium Additives. *ACS Cent. Sci.* **2017**, *3* (8), 853-859. DOI: 10.1021/acscentsci.7b00180.
(12) Thevenon, A.; Rosas-Hernández, A.; Fontani Herreros, A. M.; Agapie, T.; Peters, J. C. Dramatic HER Suppression on Ag Electrodes via Molecular Films for Highly Selective CO_2 to CO Reduction. *ACS Catal.* **2021**, *11* (8), 4530-4537. DOI: 10.1021/acscatal.1c00338.
(13) Lai, Y.; Watkins, N. B.; Muzzillo, C.; Richter, M.; Kan, K.; Zhou, L.; Haber, J. A.; Zakutayev, A.; Peters, J. C.; Agapie, T.; et al. Molecular Coatings Improve the Selectivity and Durability of CO_2 Reduction Chalcogenide Photocathodes. *ACS Energy Lett.* **2022**, *7* (3), 1195-1201. DOI: 10.1021/acsenergylett.1c02762.

(14) Tagliabue, G.; DuChene, J. S.; Abdellah, M.; Habib, A.; Gosztola, D. J.; Hattori, Y.; Cheng, W.-H.; Zheng, K.; Canton, S. E.; Sundararaman, R.; et al. Ultrafast hot-hole injection modifies hot-electron dynamics in Au/p-GaN heterostructures. *Nat. Mater.* **2020**, *19* (12), 1312-1318. DOI: 10.1038/s41563-020-0737-1.
(15) Tagliabue, G.; Jermyn, A. S.; Sundararaman, R.; Welch, A. J.; DuChene, J. S.; Pala, R.; Davoyan, A. R.; Narang, P.; Atwater, H. A. Quantifying the role of surface plasmon excitation and hot carrier transport in plasmonic devices. *Nat. Commun.* **2018**, *9* (1), 3394. DOI: 10.1038/s41467-018-05968-x.
(16) Corson, E. R.; Creel, E. B.; Kim, Y.; Urban, J. J.; Kostecki, R.; McCloskey, B. D. A temperature-controlled photoelectrochemical cell for quantitative product analysis. *Rev. Sci. Instrum.* **2018**, *89* (5), 055112. DOI: 10.1063/1.5024802.
(17) Goyal, A.; Marcandalli, G.; Mints, V. A.; Koper, M. T. M. Competition between CO_2 Reduction and Hydrogen Evolution on a Gold Electrode under Well-Defined Mass Transport Conditions. *JACS* **2020**, *142* (9), 4154-4161. DOI: 10.1021/jacs.9b10061.
(18) Xu, K.; Zhang, Q.; Zhou, X.; Zhu, M.; Chen, H. Recent Progress and Perspectives on Photocathode Materials for CO_2 Catalytic Reduction. *Nanomaterials (Basel)* **2023**, *13* (10). DOI: 10.3390/nano13101683.
(19) Buckley, A. K.; Lee, M.; Cheng, T.; Kazantsev, R. V.; Larson, D. M.; Goddard Iii, W. A.; Toste, F. D.; Toma, F. M. Electrocatalysis at Organic–Metal Interfaces: Identification of Structure–Reactivity Relationships for CO_2 Reduction at Modified Cu Surfaces. *JACS* **2019**, *141* (18), 7355-7364. DOI: 10.1021/jacs.8b13655.
(20) Chevalier, C. L.; Landis, E. C. Electrochemical Attachment of Diazonium-Generated Films on Nanoporous Gold. *Langmuir* **2015**, *31* (31), 8633-8641. DOI: 10.1021/acs.langmuir.5b02302.
(21) Yoon, Y.; Hall, A. S.; Surendranath, Y. Tuning of Silver Catalyst Mesostructure Promotes Selective Carbon Dioxide Conversion into Fuels. *Angew. Chem. Int. Ed.* **2016**, *55* (49), 15282-15286. DOI: https://doi.org/10.1002/anie.201607942.
(22) Song, D.; Lian, Y.; Wang, M.; Su, Y.; Lyu, F.; Deng, Z.; Peng, Y. Electrochemical CO_2 reduction catalyzed by organic/inorganic hybrids. *eScience* **2023**, *3* (2), 100097. DOI: https://doi.org/10.1016/j.esci.2023.100097.
(23) Hoang, T. T. H.; Ma, S.; Gold, J. I.; Kenis, P. J. A.; Gewirth, A. A. Nanoporous Copper Films by Additive-Controlled Electrodeposition: CO_2 Reduction Catalysis. *ACS Catal.* **2017**, *7* (5), 3313-3321. DOI: 10.1021/acscatal.6b03613.
(24) Ma, W.; Xie, S.; Liu, T.; Fan, Q.; Ye, J.; Sun, F.; Jiang, Z.; Zhang, Q.; Cheng, J.; Wang, Y. Electrocatalytic reduction of CO_2 to ethylene and ethanol through hydrogen-assisted C–C coupling over fluorine-modified copper. *Nat. Catal.* **2020**, *3* (6), 478-487. DOI: 10.1038/s41929-020-0450-0.
(25) Wakerley, D.; Lamaison, S.; Ozanam, F.; Menguy, N.; Mercier, D.; Marcus, P.; Fontecave, M.; Mougel, V. Bio-inspired hydrophobicity promotes CO_2 reduction on a Cu surface. *Nat. Mater.* **2019**, *18* (11), 1222-1227. DOI: 10.1038/s41563-019-0445-x.
(26) Li, F.; Thevenon, A.; Rosas-Hernández, A.; Wang, Z.; Li, Y.; Gabardo, C. M.; Ozden, A.; Dinh, C. T.; Li, J.; Wang, Y.; et al. Molecular tuning of CO_2-to-ethylene conversion. *Nature* **2020**, *577* (7791), 509-513. DOI: 10.1038/s41586-019-1782-2.
(27) Nie, W.; Heim, G. P.; Watkins, N. B.; Agapie, T.; Peters, J. C. Organic Additive-derived Films on Cu Electrodes Promote Electrochemical CO_2 Reduction to C2+ Products Under Strongly Acidic Conditions. *Angew. Chem. Int. Ed.* **2023**, *62* (12), e202216102. DOI: https://doi.org/10.1002/anie.202216102.

(28) Médard, J.; Combellas, C.; Kanoufi, F.; Pinson, J.; Chauvin, J.; Deronzier, A. Patterning Surfaces through Photografting of Iodonium Salts. *J. Phys. Chem. C* **2018**, *122* (34), 19722-19730. DOI: 10.1021/acs.jpcc.8b06541.
(29) Shinotsuka, H.; Tanuma, S.; Powell, C. J.; Penn, D. R. Calculations of electron inelastic mean free paths. X. Data for 41 elemental solids over the 50 eV to 200 keV range with the relativistic full Penn algorithm. *Surf. Interface Anal.* **2015**, *47* (9), 871-888. DOI: https://doi.org/10.1002/sia.5789.